Materials Today Physics 20 (2021) 100445

Contents lists available at ScienceDirect

Materials Today Physics

journal homepage: https://www.journals.elsevier.com/materials-today-physics

Optimizing thermal transport in graphene nanoribbon based on phonon resonance hybridization

Xiao Wan [a, b, 1], Dengke Ma [c, 1], Dongkai Pan [a, b], Lina Yang [d], Nuo Yang [a, b, *]

[a] State Key Laboratory of Coal Combustion, Huazhong University of Science and Technology, Wuhan, 430074, China
[b] School of Energy and Power Engineering, Huazhong University of Science and Technology, Wuhan, 430074, China
[c] NNU-SULI Thermal Energy Research Center (NSTER) & Center for Quantum Transport and Thermal Energy Science (CQTES), School of Physics and Technology, Nanjing Normal University, Nanjing, 210023, China
[d] School of Aerospace Engineering, Beijing Institute of Technology, Beijing, 100081, China

ARTICLE INFO

Article history:
Received 8 April 2021
Received in revised form
15 May 2021
Accepted 19 May 2021
Available online 25 May 2021

Keywords:
Graphene nanoribbon
Phonon local resonance
Thermal transport property
Atomic Green's function
Bayesian optimization

ABSTRACT

As a critical way to modulate thermal transport in nanostructures, phonon resonance hybridization has become an issue of great concern in the field of phonon engineering. In this work, we optimized phonon transport across graphene nanoribbon and obtained minimized thermal conductance by means of designing nanopillared nanostructures based on resonance hybridization. Specifically, the optimization of thermal conductance was performed by the combination of atomic Green's function and Bayesian optimization. Interestingly, it is found that thermal conductance decreases non-monotonically with the increase of number for nanopillared structure, which is severed as the resonator and blocks phonon transport. Further mode-analysis and atomic Green's function calculations revealed that the anomalous tendency originates from decreased phonon transmission in a wide frequency range. Additionally, nonequilibrium molecular dynamics simulations are performed to verify the results with the consideration of high-order phonon scattering. This finding provides novel insights into the control of phonon transport in nanostructures.

1. Introduction

Graphene nanoribbons (GNRs) have attracted great attention recently due to their extraordinary properties and potential applications in various fields [1,2]. One promising application relates to thermoelectrics [3,4]. Although the thermal conductivity of GNR is high, its mechanical flexibility and outstanding electric properties, give it potential to be applied in thermoelectrics [4]. The ability to reduce the thermal conductivity of GNR without degrading the electric properties provides a practicable avenue for improving thermoelectric performance. Besides, it's essential for understanding heat transfer physics in low-dimensional systems as well.

Tailoring thermal conductivity of materials in atomic scale through phonon engineering is a rapidly growing area of research [3,5–12]. As reported in previous works, GNRs can be synthesized from molecular precursors with atomic precision which makes it possible to manipulate their physical properties in atomic scale [13–15]. Different types of nanostructures have been proposed to reduce thermal conductivity of GNRs based on the particle nature of phonon, such as vacancies [16], edge disorders [17], and doping [18,19]. Besides, the wave nature of phonon can also be utilized to modulate thermal properties of GNR, which can be realized in nanophononic metamaterials (NPM) [3,20]. Based on local resonant hybridization, phonon transport is blocked, thus thermal conductivity can be dramatically reduced in PM, which is expected to remain excellent electric properties in the meanwhile. Previously, local resonant hybridization in silicon structures has been investigated in detail [3,20–25]. The readers are referred to a review article on NPMs [26]. By introducing nanopillars on a plate, numerous local resonances take place. Flat branches appear in the phonon dispersion, The local resonant hybridization significantly reduces the group velocities and consequently, the thermal conductivity [22].

However, the research on thermal transport properties of GNR-based nanostructures based on local resonant hybridization is relatively less. And, the development of GNR-based nanostructures with optimal thermal properties requires massive time and effort

* Corresponding author.
E-mail address: nuo@hust.edu.cn (N. Yang).
[1] X.W. and D.M. contributed equally to this work.

https://doi.org/10.1016/j.mtphys.2021.100445
2542-5293/

due to their huge parameter space. Thus, it is needed to obtain knowledge of optimal structures to guide the research by using an accelerated development process [4].

Recently, by combining material science and data science, machine learning algorithms have been widely applied in designing nanostructures and optimizing the target property [27–31]. In the field of heat conduction, the approach has been extended to the design of structures in atomic scale with optimized lattice thermal conductance or thermal conductivity [28,32,33]. These works have shown that such a method can considerably bridge the gap between structures and properties. Thus, the complex correlations among GNR-based nanostructures and their thermal properties based on phonon local resonant can be recognized utilizing machine learning algorithms, realizing structural optimization towards thermal transport properties of GNR within less property calculation.

In this work, thermal transport properties of GNRs are modulated by designing the nanopillars' arrangement. The optimization of thermal transport properties of GNRs is carried out based on the combination of Bayesian optimization (BO) and atomic Green's function (AGF), because ergodic evaluation for thermal properties of all the candidates is expensive [5,10]. Firstly, the effectiveness of the optimization method is demonstrated. Then, the optimization on GNRs with different lengths is performed. Lastly, the underlying physical mechanism is analyzed by the mode-analysis utilizing lattice dynamics. the effect of phonon scattering on the results is taken into account by performing nonequilibrium molecular dynamics (NEMD) simulations.

2. Methods

Due to phonon resonance hybridization, the introduction of nanopillar, which is served as the resonator, can have a high impact on thermal transport. How to arrange the nanopillars to obtain the largest/smallest thermal conductance? In this work, the arrangement of nanopillars on the GNR is designed to tune heat conduction in GNR based on the combination of AGF and BO. As shown in Fig. 1, the system is comprised of graphene nanoribbon and nanopillars on two sides, where nanopillars serve as resonators and the values of W, L_1, L_2, L_P, and H_P are fixed to 1.58, 1.62, 0.87, 0.62 nm, and 0.86 nm, respectively. In previous research, it has been observed that there are many flat bands in the phonon dispersion of GNRs with nanopillars in this size [19], which means that phonon local resonance takes place [3,22]. The thickness (d) of nanopillared GNRs is 0.334 nm with lattice constant (a) 0.1438 nm.

In the optimization part for thermal transport properties of nanopillared GNR, four elements are of basic requirement: the descriptor, evaluator, optimization method, and calculator. In this study, a binary flag is set as descriptors to describe the state of each nanopillar: "1" and "0" represent there is an occupied nanopillar or there is no nanopillar on the corresponding site, respectively. The thermal conductance (TC) is chosen as the evaluator for the quantitative evaluation of the performance of each candidate. Open-source Bayesian optimization library COMBO is employed to perform the optimization process [34], which has been successfully applied in recent work [4,33]. The details of Bayesian optimization can be found in the Supplemental Material (SM).

The AGF method [35–37] and NEMD simulations were utilized to calculate thermal transport properties of GNRs. Based on the Landauer formula [38], the value of TC (σ) at temperature T (300 K in this work) can be obtained by

$$\sigma = \frac{\hbar^2}{2\pi k_B T^2 S}\int \omega^2 \Xi(\omega)\frac{e^{\hbar\omega/k_BT}}{\left(e^{\hbar\omega/k_BT}-1\right)^2}d\omega \quad (1)$$

where k_B is the Boltzmann constant, ω is the phonon frequency, $\Xi(\omega)$ is the phonon transmission function calculated by AGF method and S is the cross-sectional area. The details of transmission function calculation can be found in the SM. In order to take high-order interaction into account, further NEMD simulations are conducted for validation. The Large-scale Atomic/Molecular Massively Parallel Simulation (LAMMPS) package is used in the simulations [8,39–44]. The interatomic interactions are described by the optimized Tersoff potential, which has successfully reproduced the thermal transport properties of graphene [21,45–47]. The detailed parameters and specific simulation processes are shown in the SM. Time step is set as 0.5 fs. Two Langevin thermostats [48] with a temperature difference of 20 K (310 K and 290 K) are used to establish a temperature gradient along the longitudinal direction. The thermal conductivities shown here are averaged over five independent simulations with different initial conditions.

3. Results and discussions

The optimization is divided into two steps: the first step is to testify the effectiveness of the proposed method by using a short enough nanopillared GNR, in which all of the candidates can be calculated in a short time; and the second is to apply this method to the optimization of several longer systems. In the first step, the GNR has 10 sites for nanopillars corresponding to 9.8 nm in length. So, the number of all the candidates is 2^{10} (1024). This number is small enough, so that ergodic computation can be implemented to confirm the optimization results and the efficacy of the method. Fig. 2(a) and (b) exhibit the obtained optimal structures for maximum and minimum TC for GNR, respectively.

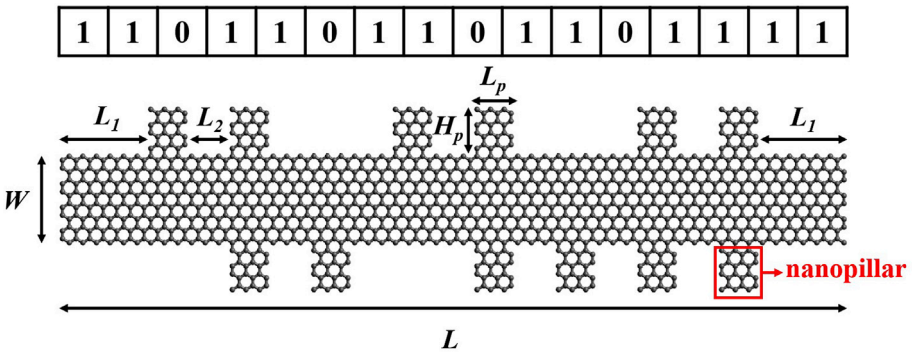

Fig. 1. Schematic picture of nanopillared GNR and corresponding binary flag.

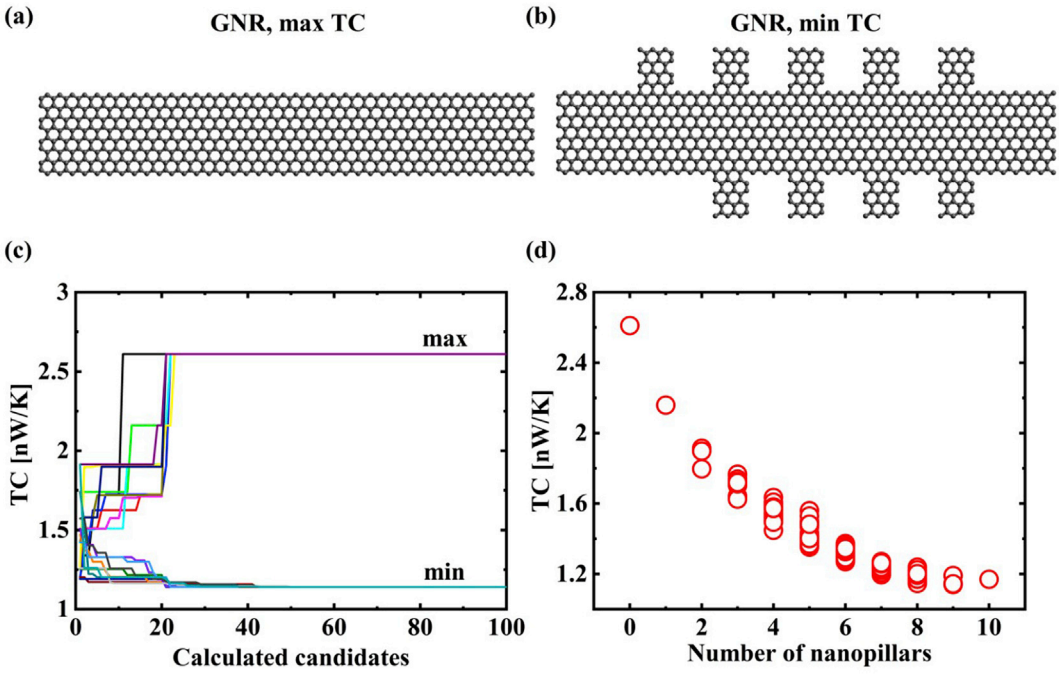

Fig. 2. (a)–(b) Optimal structures with the maximum and minimum thermal conductance for the system with the length of 9.8 nm. (c) The 10 optimization runs with different initial choices of candidates. (d) Thermal conductance versus the number of nanopillars obtained from calculations of all the candidates.

The optimal structures exhibited here are the identical results from 10 independent optimizations with different initial choices. The purpose of multi-optimization is to test the performance of Bayesian optimization algorithm. As shown in Figs. 2(c), 10 optimizations converge within calculations of 43 candidates, which is only 4.2% of all candidates. As for the accuracy of the optimization, the TCs of all candidates are calculated to verify the optimal structures, and it is confirmed that the extremum of TC (maximum and minimum) and the corresponding structures are exactly consistent with those from BO.

The distributions of TCs of all candidates with different number of nanopillars is shown in Fig. 2(d). The ratio of maximum to minimum TC is 2.3, which suggests that the TC is obviously dependent on the distribution of nanopillared nanostructure. Besides, for the structures with the same number of nanopillars, the TC values vary with the distribution of nanopillars, which indicates that phonon local resonant hybridization correlates with the site of resonators. Interestingly, the GNR with 10 sites fully occupied (1111111111) doesn't show the minimum thermal conductance, which is out of expectation. In a shorter system (with 8 sites), it is found that nanopillars enhance phonon local resonant hybridization so that the thermal conductance decreases, and when the 8 sites are fully occupied (11111111), the TC of GNR get minimum value (as shown in SM II). Since the nanopillars do not always make a negative effect on the thermal transport with the increase of the length of GNR. It is moved on to the second step and extends the optimization to several longer systems, where the number of sites is 12, 14, and 16, corresponding to 11.3, 12.8, and 14.3 nm in length, respectively. Table 1 lists the range of TC values in various total length, all the optimal structures, and the relative difference δ between the minimum TC value and the TC value of the GNR with fully occupied sites, which is defined as $\delta = (\sigma_{fo} - \sigma_{min})/\sigma_{min}$. As expected, the range of TCs is enlarged with the increase of the numbers of total candidates, where there is little variation in the maximum TC, and a little reduction in the minimum TC. The structure with the maximum TC has no nanopillars on two sides in all cases, which is understandable because the nanopillar induces phonon local resonant, blocking heat conduction. As the length of GNR increases, the structure with the minimum TC always lacks one or two nanopillars, compared with the GNR with fully occupied sites, and exhibits the aperiodicity and asymmetry. Though the difference between these two structures is very small, there is always a nonnegligible gap of thermal transport properties among them, which also enlarge in the longer GNR without convergent tendency. To be emphasized, reasonably arranging the distribution of nanopillars on the GNR can further reduce the TC on the basis of phonon local resonant.

Table 1
Optimal thermal conductance and GNR-based nanostructures obtained through Bayesian optimization for different lengths.

Length [nm]	TC [nW/K]	Optimal Structures [min/max]	δ
9.8	1.14/2.61	1111101111/0000000000	3.0%
11.3	1.07/2.62	111101101111/000000000000	6.5%
12.8	1.03/2.63	110111111101111/000000000000000	9.7%
14.3	0.99/2.63	0111111111110111/0000000000000000	12.1%

Now that the structures with the minimum TC are identified, the mechanisms behind the smaller TC need to be investigated. Firstly, phonon dispersion relations of the GNR with fully occupied sites and the GNR with the minimum TC are compared. As a representative instance, the longest system (16 sites, 14.3 nm) is investigated in detail, where three structures are chosen for comparison: the GNR with the maximum TC (0000000000000000), the GNR with the minimum TC (0111111111110111), and the GNR with fully occupied sites (1111111111111111).

The phonon dispersion relationship and phonon transmission function are shown in Fig. 3(a) and (b), respectively. Compared to the GNR (0000000000000000), the other two GNRs (0111111111110111 and 1111111111111111) exhibit many additional flat bands in the phonon dispersion, which means phonon local resonance at corresponding frequencies [3]. More resonant modes

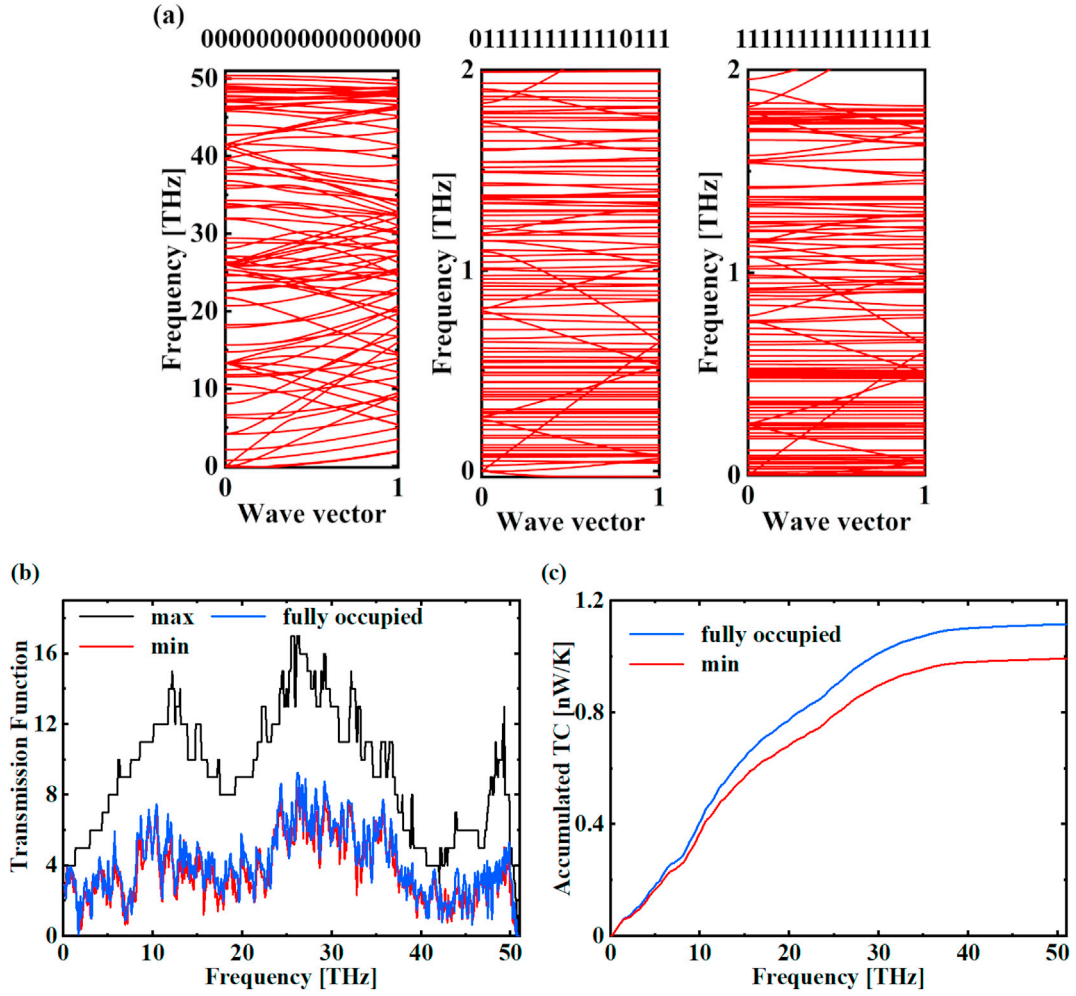

Fig. 3. The total length of the system in this case is fixed as 14.3 nm. (a) The phonon dispersion relationship of the GNRs with the maximum TC, the minimum TC, and fully occupied sites, respectively. (b) The phonon transmission function of these three structures. (c) The accumulated thermal conductance of the GNRs with the minimum TC and fully occupied sites.

will induce more hybridization and impede phonon transport, which leads to the decrease of group velocities [3,19]. For the GNRs (0111111111110111) and (1111111111111111), although their TC values differ by 12.1%, the difference in their phonon dispersion is very small, which is not obvious in Fig. 3(a). To better show the difference, the transmission function and accumulated thermal conductance of these three structures are calculated and shown in Fig. 3(b), where the resonant modes can be recognized from the first transmission function minimum (at 1.67 THz). The transmission function of pristine GNR (0000000000000000) is much higher than those of the latter two structures over a wide frequency range. More importantly, the GNR with the minimum TC exhibits the lower TC due to the lower transmission function in the frequency of 10–40 THz. This implies that it is by arranging the distribution of fixed-size nanopillars on the base-structure that phonon transport could be blocked in a wide frequency range, even though the single nanopillar with fixed size can only hybridize some phonon modes at a certain frequency.

Considering effects of nanopillar density on heat conduction in a graphene nanoribbon, there are competing effects when increasing of nanopillars. More nanopillars can block more phonon transport by inducing more resonant hybridization. However, at the same time, dense nanopillars could enhance phonon coherence, which takes a larger thermal conductance [49,50]. Thus, the competitive effects bring a minimum value of thermal conductance as the increasing of nanopillar density. Once removing a few nanopillars from the graphene nanoribbon with fully occupied sites, there might be less phonon coherence, hence exhibiting a smaller thermal conductance.

To further expand the above-discussed conclusions to more realistic systems, NEMD is utilized in consideration of phonon-phonon scattering. The thermal conductivities of the GNRs with the minimum TC in different total length L are calculated, and compared with the thermal conductivities of corresponding GNRs with fully occupied sites. Besides, the thermal conductivities of GNRs with no nanopillars that always exhibit the highest TC among different lengths (9.8, 11.3, 12.8, and 14.3 nm) are also studied to test size effect. The thermal conductivity values of these structures are 228.13 ± 11.88, 264.00 ± 14.63, 314.73 ± 16.68, 344.41 ± 10.83 W/m-K, respectively.

Obviously, thermal conduction is a function of length, which is because the phonon transport is largely affected by the boundary scattering, when the size of structures is comparable with the phonon mean free path [10]. As shown in Fig. 4, the GNR with the minimum TC also exhibits lower thermal conductivity compared with the GNR with fully occupied sites in different systems. Furthermore, the difference of thermal conductivities among these two structures also increases with the length of the whole system.

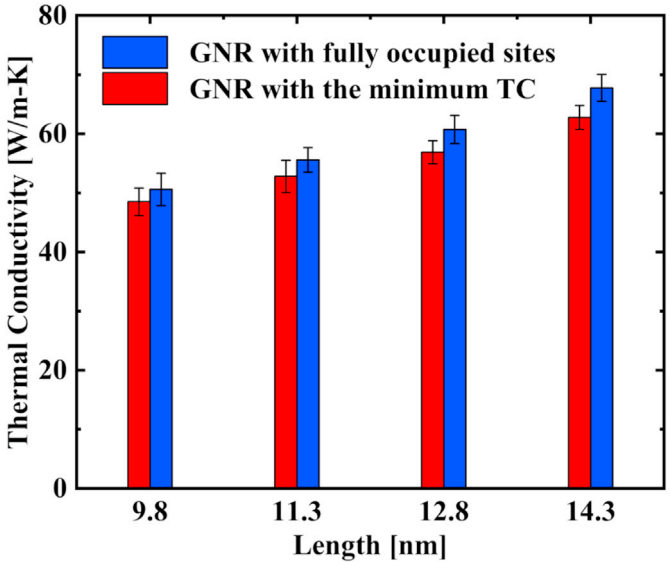

Fig. 4. Thermal conductivities of the GNRs with fully occupied sites and the minimum TC among different total length *L* obtained from NEMD.

It is indicated that the introduction of phonon scattering does not impact the inferences based on phonon local resonance above.

4. Conclusions

In summary, we optimize thermal transport properties of nanopillared GNR based on phonon local resonances, by identifying the structures with the minimum or maximum TC. It is interesting that although the nanopillar can introduce phonon local resonant hybridization wave effect to block thermal transport, the GNR with fully occupied sites does not exhibit the lowest TC. This phenomenon becomes more obvious as the length of the whole system increases. According to AGF calculation and phonon mode analysis, it is concluded that arranging the distribution of resonators on the base-structure could block phonon transport in a wide frequency range, even though the size of them doesn't change, which means the resonant modes remain the same. In the end, we perform NEMD to confirm the results above in consideration of phonon scattering, which is consistent with AGF calculations.

Here, it shows that the design of minimum or maximum thermal conductance is not by monotonic adjusting the density of nanopillars. Because there are competing effects when the density of nanopillars is high. Hence, to achieve the minimized thermal transport properties, machine learning algorithms could be an effective way to find an optimized design that generally is aperiodicity and asymmetry. It paves a new way for manipulating phonon transport in nanostructures.

Credit author statement

Xiao Wan: Conceptualization, Methodology, Formal analysis, Investigation, Writing – original draft. Dengke Ma: Methodology, Investigation, Formal analysis, Writing – original draft. Dongkai Pan: Investigation, Formal analysis. Lina Yang: Investigation, Formal analysis. Nuo Yang: Conceptualization, Supervision, Writing - Original Draf, Funding acquisition.

Declaration of competing interest

The authors declare that they have no known competing financial interests or personal relationships that could have appeared to influence the work reported in this paper.

Acknowledgements

This work is sponsored by the National Key Research and Development Project of China No. 2018YFE0127800, National Natural Science Foundation of China No. 12005105, Fundamental Research Funds for the Central Universities No. 2019kfyRCPY045 and Program for HUST Academic Frontier Youth Team. We are grateful to Shiqian Hu, Meng An, Xiaoxiang Yu, Wentao Feng and Han Meng for useful discussions. The authors thank the National Supercomputing Center in Tianjin (NSCC-TJ) and the China Scientific Computing Grid (ScGrid) for providing assistance in computations.

Appendix A. Supplementary data

Supplementary data to this article can be found online at https://doi.org/10.1016/j.mtphys.2021.100445.

References

[1] X. Yu, H. Cheng, M. Zhang, Y. Zhao, L. Qu, G. Shi, Nature Reviews Materials 2 (2017) 17046.
[2] M. Yankowitz, Q. Ma, P. Jarillo-Herrero, B.J. LeRoy, Nature Reviews Physics 1 (2019) 112.
[3] B.L. Davis, M.I. Hussein, Phys. Rev. Lett. 112 (2014): 055505.
[4] M. Yamawaki, M. Ohnishi, S. Ju, J. Shiomi, Science Advances 4 (2018) eaar4192.
[5] N. Yang, X. Xu, G. Zhang, B. Li, AIP Adv. 2 (2012): 041410.
[6] D.G. Cahill, et al., Appl. Phys. Rev. 1 (2014): 011305.
[7] J. Kaiser, T. Feng, J. Maassen, X. Wang, X. Ruan, M. Lundstrom, J. Appl. Phys. 121 (2017): 044302.
[8] C. Deng, Y. Huang, M. An, N. Yang, Materials Today Physics 16 (2021) 100305.
[9] B. Liao, G. Chen, MRS Bull. 40 (2015) 746.
[10] N. Li, J. Ren, L. Wang, G. Zhang, P. Hänggi, B. Li, Rev. Mod. Phys. 84 (2012) 1045.
[11] H. Meng, M. An, T. Luo, N. Yang, in: X. Liu, et al. (Eds.), Chalcogenide, Woodhead Publishing, 2020, p. 31.
[12] M. An, H. Meng, T. Luo, N. Yang, in: X. Liu, et al. (Eds.), Chalcogenide, Woodhead Publishing, 2020, p. 339.
[13] L. Talirz, et al., ACS Nano 11 (2017) 1380.
[14] J. Cai, et al., Nature 466 (2010) 470.
[15] Y.-C. Chen, T. Cao, C. Chen, Z. Pedramrazi, D. Haberer, D.G. de Oteyza, F.R. Fischer, S.G. Louie, M.F. Crommie, Nat. Nanotechnol. 10 (2015) 156.
[16] J. Haskins, A. Kınacı, C. Sevik, H. Sevinçli, G. Cuniberti, T. Çağın, ACS Nano 5 (2011) 3779.
[17] H. Sevinçli, G. Cuniberti, Phys. Rev. B 81 (2010) 113401.
[18] S. Chen, Q. Wu, C. Mishra, J. Kang, H. Zhang, K. Cho, W. Cai, A.A. Balandin, R.S. Ruoff, Nat. Mater. 11 (2012) 203.
[19] D. Ma, X. Wan, N. Yang, Phys. Rev. B 98 (2018) 245420.
[20] S. Xiong, D. Selli, S. Neogi, D. Donadio, Phys. Rev. B 95 (2017) 180301.
[21] D. Ma, H. Ding, H. Meng, L. Feng, Y. Wu, J. Shiomi, N. Yang, Phys. Rev. B 94 (2016) 165434.
[22] S. Xiong, K. Sääskilahti, Y.A. Kosevich, H. Han, D. Donadio, S. Volz, Phys. Rev. Lett. 117 (2016): 025503.
[23] H. Honarvar, L. Yang, M.I. Hussein, Appl. Phys. Lett. 108 (2016) 263101.
[24] H. Honarvar, M.I. Hussein, Phys. Rev. B 97 (2018) 195413.
[25] H. Wang, Y. Cheng, M. Nomura, S. Volz, D. Donadio, X. Zhang, S. Xiong, Phys. Rev. B 103 (2021): 085414.
[26] M.I. Hussein, C.-N. Tsai, H. Honarvar, Adv. Funct. Mater. 30 (2020) 1906718.
[27] K. Rajan, Mater. Today 8 (2005) 38.
[28] X. Wan, W. Feng, Y. Wang, H. Wang, X. Zhang, C. Deng, N. Yang, Nano Lett. 19 (2019) 3387.
[29] T. Wang, C. Zhang, H. Snoussi, G. Zhang, Adv. Funct. Mater. 30 (2020) 1906041.
[30] T. Wang, M. Shao, R. Guo, F. Tao, G. Zhang, H. Snoussi, X. Tang, Adv. Funct. Mater. 31 (2021) 2006245.
[31] L. Yang, X. Wan, D. Ma, Y. Jiang, N. Yang, Phys. Rev. B 103 (2021) 155305.
[32] H. Wei, H. Bao, X. Ruan, Nanomater. Energy 71 (2020) 104619.
[33] S. Ju, T. Shiga, L. Feng, Z. Hou, K. Tsuda, J. Shiomi, Phys. Rev. X 7 (2017): 021024.
[34] T. Ueno, T.D. Rhone, Z. Hou, T. Mizoguchi, K. Tsuda, Materials Discovery 4 (2016) 18.
[35] J.S. Wang, J. Wang, J.T. Lü, The European Physical Journal B 62 (2008) 381.
[36] Z. Tian, K. Esfarjani, G. Chen, Phys. Rev. B 86 (2012) 235304.
[37] S. Hu, L. Feng, C. Shao, I.A. Strelnikov, Y.A. Kosevich, J. Shiomi, Phys. Rev. B 102 (2020): 024301.
[38] R. Landauer, Phil. Mag. 21 (1970) 863.

[39] M. An, L. Li, S. Hu, Z. Ding, X. Yu, B. Demir, N. Yang, W. Ma, X. Zhang, Carbon 162 (2020) 202.
[40] H. Meng, D. Ma, X. Yu, L. Zhang, Z. Sun, N. Yang, Int. J. Heat Mass Tran. 145 (2019) 118719.
[41] H. Meng, X. Yu, H. Feng, Z. Xue, N. Yang, Int. J. Heat Mass Tran. 137 (2019) 1241.
[42] S. Plimpton, J. Comput. Phys. 117 (1995) 1.
[43] X. Yu, R. Li, T. Shiga, L. Feng, M. An, L. Zhang, J. Shiomi, N. Yang, J. Phys. Chem. C 123 (2019) 26735.
[44] S. Deng, J. Yuan, Y. Lin, X. Yu, D. Ma, Y. Huang, R. Ji, G. Zhang, N. Yang, Nanomater. Energy 82 (2021) 105749.
[45] S. Hu, S. Ju, C. Shao, J. Guo, B. Xu, M. Ohnishi, J. Shiomi, Materials Today Physics 16 (2021) 100324.
[46] M. An, Q. Song, X. Yu, H. Meng, D. Ma, R. Li, Z. Jin, B. Huang, N. Yang, Nano Lett. 17 (2017) 5805.
[47] L. Lindsay, D.A. Broido, Phys. Rev. B 81 (2010) 205441.
[48] T. Ouyang, Y.P. Chen, K.K. Yang, J.X. Zhong, Europhys. Lett. 88 (2009) 28002.
[49] S. Hu, Z. Zhang, P. Jiang, W. Ren, C. Yu, J. Shiomi, J. Chen, Nanoscale 11 (2019) 11839.
[50] S. Hu, Z. Zhang, P. Jiang, J. Chen, S. Volz, M. Nomura, B. Li, J. Phys. Chem. Lett. 9 (2018) 3959.

Supplemental Material

Optimizing Thermal Transport in Graphene Nanoribbon Based on Phonon Resonance Hybridization

Xiao Wan[1,2#], Dengke Ma[3#], Dongkai Pan[1,2], Lina Yang[4], Nuo Yang[1,2*]

1. State Key Laboratory of Coal Combustion, Huazhong University of Science and Technology, Wuhan 430074, China.

2. School of Energy and Power Engineering, Huazhong University of Science and Technology, Wuhan 430074, China.

3. NNU-SULI Thermal Energy Research Center (NSTER) & Center for Quantum Transport and Thermal Energy Science (CQTES), School of Physics and Technology, Nanjing Normal University, Nanjing 210023, China.

4. School of Aerospace Engineering, Beijing Institute of Technology, Beijing 100081, China.

# X.W. and D.M. contributed equally to this work.

*Corresponding email: nuo@hust.edu.cn (N.Y)

SM I. Molecular dynamics simulation details

<table>
<tr><td>Method</td><td colspan="6">Non-equilibrium MD</td></tr>
<tr><td colspan="7">Potential (TERSOFF)</td></tr>
<tr><td>Function</td><td colspan="6">$$E = \frac{1}{2}\sum_i \sum_{j(\neq i)} f_C(r_{ij})\left[f_R(r_{ij}) + b_{ij} f_A(r_{ij})\right]$$
$$f_C(r) = \begin{cases} 1 : r < R - D \\ \frac{1}{2} - \frac{1}{2} sin\left(\frac{\pi}{2}\frac{r-D}{D}\right) : R - D < r < R + D \\ 0 : r > R + D \end{cases}$$
$$f_R(r) = Aexp(-\lambda_1 r) \;\; f_A(r) = -Bexp(-\lambda_2 r)$$
$$b_{ij} = \left(1 + \beta^n \varsigma_{ij}^n\right)^{-\frac{1}{2n}}$$
$$\varsigma_{ij} = \sum_{k \neq i,j} f_C(r_{ij}) g(\theta_{ijk}) exp\left[\lambda_3^m (r_{ij} - r_{ik})^m\right]$$
$$g(\theta) = \gamma_{ijk}\left(1 + \frac{c^2}{d^2} - \frac{c^2}{[d^2 + (cos\theta - cos\theta_0)^2]}\right)$$</td></tr>
<tr><td rowspan="2">Parameters</td><td>m</td><td>γ</td><td>λ</td><td>c</td><td>d</td><td>cosθ</td></tr>
<tr><td>3.0</td><td>1.0</td><td>3.8e4</td><td>4.3484</td><td>-0.930</td><td>0.72751</td></tr>
<tr><td>n</td><td>β</td><td>λ</td><td>B</td><td>R</td><td>λ</td><td>A</td></tr>
<tr><td>1.57e-7</td><td>2.2119</td><td>430.0</td><td>1.95</td><td>0.15</td><td>3.4879</td><td>1393.6</td></tr>
<tr><td colspan="7">Simulation process</td></tr>
<tr><td>Ensemble</td><td colspan="3">Setting</td><td colspan="3">Purpose</td></tr>
<tr><td rowspan="3">NPT</td><td colspan="2">Runtime (ns)</td><td colspan="2">1</td><td colspan="2" rowspan="5">Relax structure</td></tr>
<tr><td colspan="2">Temperature (K)
Pressure (bars)</td><td colspan="2">300
0</td></tr>
<tr><td colspan="2">Boundary condition</td><td colspan="2">longitudinal, transverse, periodic, periodic</td></tr>
<tr><td rowspan="2">NVE</td><td colspan="2">Runtime (ns)</td><td colspan="2">1.5</td></tr>
<tr><td colspan="2">Boundary condition</td><td colspan="2">longitudinal, transverse, fixed, free</td></tr>
</table>

<table>
<tr><td rowspan="2"></td><td rowspan="2">Thermostat</td><td>Heat source</td><td>310 K</td><td rowspan="2"></td></tr>
<tr><td>Heat sink</td><td>290 K</td></tr>
<tr><td rowspan="5">NVE</td><td>Runtime (ns)</td><td colspan="2">10</td><td rowspan="5">Record information</td></tr>
<tr><td>Boundary condition</td><td colspan="2">longitudinal, transverse, fixed, free</td></tr>
<tr><td rowspan="3">Thermostat</td><td>Heat source</td><td>310 K</td></tr>
<tr><td>Heat sink</td><td>290 K</td></tr>
<tr><td colspan="5"></td></tr>
<tr><td colspan="5">Recorded physical quantity</td></tr>
<tr><td colspan="2">Temperature</td><td colspan="3">$\langle E \rangle = \sum_{i=1}^{N} \frac{1}{2} m v_i^2 = \frac{1}{2} N k_B T_{MD}$</td></tr>
<tr><td colspan="2">Heat flux</td><td colspan="3">$J = \frac{1}{N_t} \sum_{i=1}^{N_t} \frac{\Delta \varepsilon_i}{2 \Delta t}$</td></tr>
<tr><td colspan="2">Thermal conductivity</td><td colspan="3">$\kappa = -\frac{J}{W \cdot d \cdot \nabla T}$</td></tr>
</table>

SM II. Thermal conductivity calculation

In the simulation, the nanopillared GNR is divided into N layers along the longitudinal direction. The system is coupled with Langevin thermostats at the 3rd to 6th and (N-5) th to (N-2) th layers with 310 and 290 K, respectively. Atoms at the boundaries (the 1st to 2nd and (N−1) th to N th layers) are fixed. The equations of motions are integrated by the velocity Verlet method. The temperature gradient is obtained by linear fitting to the local temperature, excluding the temperature jumps at two ends. As shown in SM I, the thermal conductivity is calculated based on the Fourier's Law, where J denotes the heat current transported from the heat bath to the heat sink, which is recorded by the average of the energy input and output rates from two baths. The energy and temperature profiles at steady state are shown in **Fig. S1**.

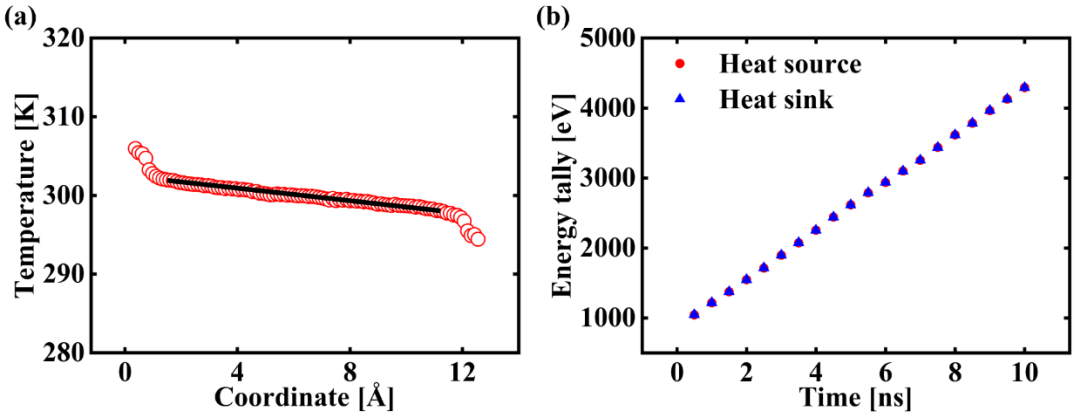

Fig. S1. (a) Steady-state temperature profile of GNR with the maximum thermal conductance obtained using the NEMD simulations at 300 K for the system length L = 12.8 nm. The black line is the fitting curve, and its slope is the temperature gradient used for calculating thermal conductivity. (b) Energies added to the hot bath and removed from the cold bath with respect to the time.

SM III. Bayesian optimization

Bayesian optimization (BO), which acts as a very effective global optimization algorithm compared with other machine learning optimization methods, has been widely applied in designing problems. It can guarantee to obtain the optimal solution under a few numbers of function evaluations due to its sophisticated prediction algorithm. In this work, the optimization problem is how to arrange the nanopillars on the graphene nanoribbon (GNR) to obtain the maximum and minimum thermal conductance (TC). Basic setting has been described in the Methods part. We employ open-source Bayesian optimization library COMBO to perform the optimization process. As shown in **Fig. S2. (a)**, suppose that TCs of *n* candidates are initially calculated, and we are to choose the next one to calculate. A Bayesian regression function is learned from n pairs of descriptors and thermal conductance (i.e., training examples). For each of the remaining candidates, a predictive distribution of thermal conductance is estimated. The best candidate is chosen based on the criterion of expected improvement. Finally, thermal conductance is calculated for the chosen candidate, and it is added to the training examples. By repeating this procedure, the calculation of thermal conductance is scheduled optimally, and the best candidate can be found quickly. The specific mathematic process is elaborated in the Ref. [Mater. Discovery 4, 18 (2016)].

Taking the GNR having 8 sites for different nanopillars corresponding to 8.3 nm in length as an example, 10 rounds of optimization are conducted with different initial choices of 20 candidates. As shown in **Fig. S2. (a)**, all optimizations come to convergence within calculations of 30 structures, which is only 11.7% of the total number of candidates (256, 8 sites). To check the accuracy of the optimization, the TCs of all candidates are also calculated, and the maximum and minimum TC and the corresponding structures are confirmed to be exactly the same as those obtained by Bayesian optimization. The distributions of TCs obtained by calculation of all the candidates with different number of nanopillars is shown in **Fig. S2. (b)**, which also confirms the accuracy of those optimizations. It is also found that nanopillars enhance

phonon local resonant hybridization so that the thermal conductance decreases, and when the sites are fully occupied on the GNR, the TC get minimum value.

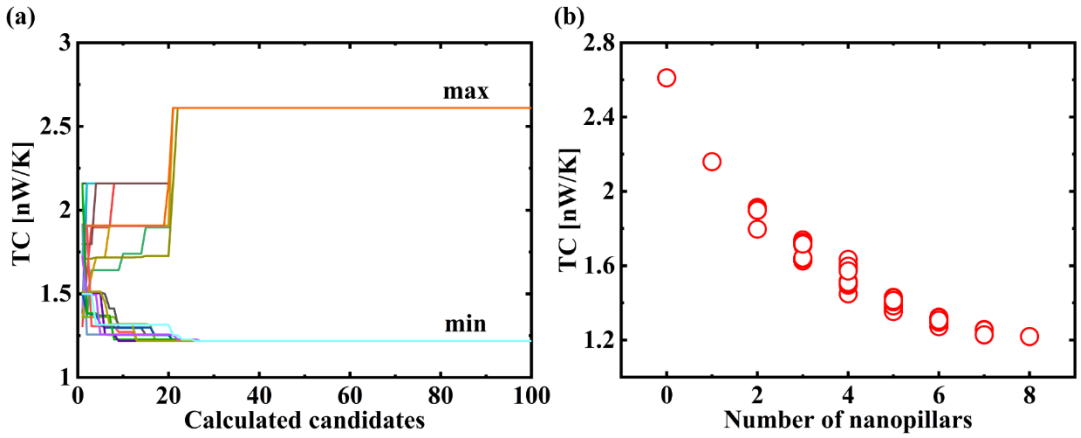

Fig. S2. The total length of the system in this case is fixed as 8.3 nm. (a) The 10 optimization runs with different initial choices of candidates. (b) Thermal conductance versus number of nanopillars obtained from calculations of all the candidates.

SM IV. Atomic Green's function

The atomic Green's function method was employed to calculate the phonon transmission function $\Xi(\omega)$

$$\Xi(\omega)=\mathrm{Tr}[\Gamma_L G^r \Gamma_R G^a] \quad (1)$$

where ω is the phonon frequency, G^r and G^a are the retarded and advanced Green functions of the scattering region, which can be expressed as

$$G^r = [(\omega + i\eta)^2 I - K^C - \Sigma_L^r - \Sigma_R^r]^{-1} \quad (2)$$

The level broadening matrices Γ_L and Γ_R describe the rates of inflow from the left lead and outflow into the right lead, which can be expressed as

$$\Gamma_L = i(\Sigma_L^r - \Sigma_L^a),\ \Gamma_R = i(\Sigma_R^r - \Sigma_R^a) \quad (3)$$

where K^C is the force constant matrix of the scattering region. Σ_L and Σ_R are the self-energies, which are calculated from surface Green's functions of left and right leads, respectively.